

RESEARCH ARTICLE

10.1002/2015JG003184

Key Points:

- CH₄ emissions from Arctic lakes will rise substantially in the 21st century
- Most of the emitted CH₄ originates from nonpermafrost carbon stock
- The increased CH₄ emissions will mainly be a consequence of lake sediments warming

Supporting Information:

- Supporting Information S1

Correspondence to:

Q. Zhuang,
qzhuang@purdue.edu

Citation:

Tan, Z., and Q. Zhuang (2015), Methane emissions from pan-Arctic lakes during the 21st century: An analysis with process-based models of lake evolution and biogeochemistry, *J. Geophys. Res. Biogeosci.*, 120, doi:10.1002/2015JG003184.

Received 15 AUG 2015

Accepted 3 DEC 2015

Accepted article online 9 DEC 2015

Methane emissions from pan-Arctic lakes during the 21st century: An analysis with process-based models of lake evolution and biogeochemistry

Zeli Tan^{1,2} and Qianlai Zhuang^{1,2,3}

¹Department of Earth, Atmospheric, and Planetary Sciences, Purdue University, West Lafayette, Indiana, USA, ²Purdue Climate Change Research Center, Purdue University, West Lafayette, Indiana, USA, ³Department of Agronomy, Purdue University, West Lafayette, Indiana, USA

Abstract The importance of methane emissions from pan-Arctic lakes in the global carbon cycle has been suggested by recent studies. These studies indicated that climate change influences this methane source mainly in two ways: the warming of lake sediments and the evolution of thermokarst lakes. Few studies have been conducted to quantify the two impacts together in a unified modeling framework. Here we adapt a region-specific lake evolution model to the pan-Arctic scale and couple it with a lake methane biogeochemical model to quantify the change of this freshwater methane source in the 21st century. Our simulations show that the extent of thaw lakes will increase throughout the 21st century in the northern lowlands of the pan-Arctic where the reworking of epigenetic ice in drained lake basins will continue. The projected methane emissions by 2100 are $28.3 \pm 4.5 \text{ Tg CH}_4 \text{ yr}^{-1}$ under a low warming scenario (Representative Concentration Pathways (RCPs) 2.6) and $32.7 \pm 5.2 \text{ Tg CH}_4 \text{ yr}^{-1}$ under a high warming scenario (RCP 8.5), which are about 2.5 and 2.9 times the simulated present-day emissions. Most of the emitted methane originates from nonpermafrost carbon stock. For permafrost carbon, the methanogenesis will mineralize a cumulative amount of $3.4 \pm 0.8 \text{ Pg C}$ under RCP 2.6 and $3.9 \pm 0.9 \text{ Pg C}$ under RCP 8.5 from 2006 to 2099. The projected emissions could increase atmospheric methane concentrations by 55.0–69.3 ppb. This study further indicates that the warming of lake sediments dominates the increase of methane emissions from pan-Arctic lakes in the future.

1. Introduction

Methane (CH₄) is the second most potent carbon-based greenhouse gas in the Earth's atmosphere and accounts for 20% of the total radiative forcing induced by the long-lived greenhouse gases [Myhre et al., 2013]. With the outburst of anthropogenic emissions, perhaps exacerbated by natural emissions, the average concentration of CH₄ in the atmosphere has risen by about 150% since 1750 [Dlugokencky et al., 2011]. Although major CH₄ sources (wetlands, rice paddies, landfills, fossil fuels, and ruminants) have been identified [Andreae and Merlet, 2001], we still lack complete understanding of some natural CH₄ sources which are important for the global CH₄ cycle. Recent investigations have identified significant amounts of CH₄ emitted from inland water systems including lakes, reservoirs, rivers, and streams, which have not been incorporated into the CH₄ inventory [Louis et al., 2000; Bastviken et al., 2004, 2011; Campeau et al., 2014; Sawakuchi et al., 2014]. For example, Bastviken et al. [2011] estimated that global lakes alone could emit CH₄ as much as 103 Tg yr^{-1} , nearly a half of the contribution from global wetlands. In particular, CH₄ emissions from pan-Arctic lakes were suggested to be much stronger than previously claimed and sensitive to the fast change of climate in the Arctic region [Zimov et al., 1997; Walter et al., 2006, 2008; Kirtman et al., 2013; Wik et al., 2014; Thornton et al., 2015].

CH₄ production in pan-Arctic thermokarst lakes can be stimulated by the warming of lake sediments and the erosion of permafrost carbon. Because these thermokarst lakes are usually shallow [Kirpotin et al., 2008; West and Plug, 2008; Manasypov et al., 2015], they are more sensitive to the changes of local air temperature and precipitation than deep lakes [Thornton et al., 2015]. And with more energy entering the lake sediments, the mobilized labile permafrost carbon could be rapidly mineralized in anoxic conditions, sustaining high CH₄ fluxes [Zimov et al., 1997; Walter et al., 2006; Spencer et al., 2015]. The permafrost zone hydrology can also change dramatically in the future due to the warming-induced degradation of permafrost, which can increase or decrease thermokarst depressions (e.g., thermokarst lakes) [Yoshikawa and Hinzman, 2003; Smith et al., 2005; Riordan et al., 2006; Avis et al., 2011]. As a result, CH₄ emissions from these lakes could rise or fall dramatically.

Although these two changes have been studied separately, they have not been quantified together in a unified process-based modeling framework [van Huissteden *et al.*, 2011; Gao *et al.*, 2013].

To fill this gap, we couple a pan-Arctic scale lake evolution model with a process-based lake biogeochemical model to quantify the CH₄ emissions from pan-Arctic lakes during the 21st century. The developed lake evolution model simulates the whole life cycle of thermokarst lakes explicitly, including (1) the ice-rich permafrost degradation initiated by climate change or surface disturbance, (2) the development of small thaw ponds following ground subsidence, (3) the expansion of thaw ponds by surface and subsurface thawing, (4) the expansion into large lakes by bank erosion and subsurface thawing, (5) the partial or complete drainage by stream capture or breaching, and (6) the resettlement of ice wedges at the bottom of drained basins [Everett, 1980; Shirokova *et al.*, 2009]. With this coupled model system, we can quantify the following: (1) to what extent the distribution and abundance of thermokarst lakes in the circum-Arctic region will be shifted due to climate change, (2) the spatial and temporal variability of CH₄ emissions from pan-Arctic lakes under changing landscape conditions, and (3) to what extent the mobilized permafrost carbon will be mineralized via methanogenesis, during the 21st century.

2. Methods

2.1. Model Description

To assess the impact of global warming on the abundance of pan-Arctic thaw lakes, we adapt a landscape evolution model described by van Huissteden *et al.* [2011] from a regional scale (several hundred square kilometers) to a continental scale (high-latitude lands north of 60°N). This northern high-latitude landscape evolution model (NHLEM) consists of all processes in the original model, including (1) thaw lake initialization on ice-rich permafrost driven by high summer temperature and annual precipitation; (2) thaw lake expansion to neighboring icy permafrost pixels driven by high summer temperature, high annual precipitation, and wind; (3) thaw lake drainage owing to connection with rivers, streams, and drained basins; and (4) drained basin refreezing due to frost heave when annual air temperature is below -7°C . The main adaptation of the NHLEM model is to initialize the landscape and ground ice conditions of land pixels in the model with data of topography, permafrost, soil, and drainage networks. The modeling study of van Huissteden *et al.* [2011] was for the Indigirka lowlands, northeast Siberia, where topography is relatively homogeneous and the distribution of ground ice content and drainage systems is known from intense investigations. Here we assume that thermokarst lakes can only develop on nonsandy (silt- or clay-rich soils) ice-rich lowland permafrost zones [Allard *et al.*, 1996; Jorgenson and Shur, 2007; Smith *et al.*, 2007; McGuire, 2013; Bouchard *et al.*, 2014]. The permafrost extent of the pan-Arctic is extracted from a 12.5 km resolution Circum-Arctic Map of Permafrost and Ground Ice Conditions database [Brown *et al.*, 2002]. This database also provides information about the abundance and content of ground ice in the upper 20 m permafrost [Lee *et al.*, 2014]. Permafrost soil is identified as nonsandy only when its sand fraction is less than 50%. The texture information of permafrost soils is retrieved from a 30 arc sec resolution (approximately 1 km) soil texture map in Harmonized World Soil Database version 1.2 [FAO/IIASA/ISRIC/ISSCAS/JRC, 2012]. The distribution of lowlands (Figure S1 in the supporting information) is produced from a global digital elevation model GTOPO30 with a horizontal grid spacing of 30 arc sec and a geographic database HYDRO1K. We define “lowland” terrains as land pixels with the standard deviation of the log-transformed elevation (ESD) less than 1.179 and the compound topographic index (CTI) larger than 6.146 [McGuire, 2013]. The ESD and CTI of land pixels are derived from GTOPO30 and HYDRO1K, respectively. For areas where CTI data are not available (e.g., Greenland), lowland terrains are identified using the criteria (elevation less than 300 m above sea level) of Smith *et al.* [2007]. Chen *et al.* [2013] showed that the connectivity between lakes and rivers is an important factor for controlling the dynamics of thermokarst lakes in permafrost zones. In the NHLEM model, multiple drainage systems are included: rivers, streams, floodplains, drained basins, coastlines, permafrost-free lowlands, and nonthermokarst lakes. The distribution of drained basins is simulated using the model, and the distribution of other drainage systems is assumed to be static and retrieved from several geographical data sets. The channels of rivers and streams are extracted from the streamline data layer distributed with HYDRO1K. The coverage of floodplains is identified from the Global Lakes and Wetlands Database (GLWD) [Lehner and Döll, 2004]. Both nonthermokarst water bodies and permafrost-free lowlands are inferred from the Circum-Arctic Map of Permafrost and Ground Ice Conditions database. The distribution of yedoma permafrost is retrieved from the geospatial maps of late Pleistocene age ice-rich syngenetic yedoma permafrost in east and central Siberia and North America [Wolfe *et al.*, 2009; Grosse *et al.*, 2013b].

The lake biogeochemical model (bLake4Me) used in this study has been detailed in *Tan et al.* [2015]. This one-dimensional process-based climate-sensitive model consists of a water thermal module, a sediment thermal module, a sediment biogeochemical module, a water column biogeochemical module, and a bubble transport module [Tan et al., 2015]. The bLake4Me model parameterizes anaerobic CH₄ production in sediments (methanogenesis) and aerobic CH₄ consumption in oxygenated water (methanotrophy) as functions of substrate availability and temperature. The dynamics of dissolved N₂ and CH₄ in lake sediments and of dissolved N₂, O₂, CO₂, and CH₄ in lake water columns are also included. In nonyedoma thermokarst lakes and nonthermokarst lakes, methanogens are fed by the decomposition of recalcitrant carbon at surface sediments only [Tan et al., 2015]. In yedoma thermokarst lakes, methanogenesis is also stimulated by the mineralization of the mobilized permafrost carbon at deep sediments. As illustrated by *Tan and Zhuang* [2015], this biogeochemical model is capable of simulating CH₄ emissions from pan-Arctic lakes with the proper configuration of environment conditions, such as organic carbon density and yedoma and nonyedoma permafrost extent. One main limitation of the method of *Tan and Zhuang* [2015] is the lack of quantifying the uncertainty of the model simulations induced by the uncertain biogeochemistry-related parameters that were obtained from only a small amount of field data [Tan et al., 2015]. The difficulty is that to quantify the uncertainty, a large number of model simulations need to be conducted for over 1.7 million lake pixels.

In our previous work, several geographic data sets were used to identify the extent and bathymetry of thermokarst lakes in the pan-Arctic [Tan and Zhuang, 2015]. As discussed, this method could cause large uncertainties of the simulated CH₄ fluxes because the depth and talik thickness information of many small Arctic thaw lakes are missed in the 1 km resolution lake database [Tan and Zhuang, 2015]. With the development of the NHLEM model, we can now simulate the extent and age of thermokarst lakes directly. We can also calculate the depth and talik thickness of each of the modeled lakes using a two-dimensional conductive heat transfer model described by *West and Plug* [2008]. This heat transfer model is driven with air temperature, soil ice content, and ground ice thickness [West and Plug, 2008]. As described by *West and Plug* [2008], the increase of water depth in a thaw lake depends on the development of its talik thickness and the conditions of soil ice content and ground ice thickness. For nonthermokarst lakes, we do not deal with their evolutions in the NHLEM model, instead assuming their extent to be constant throughout the 21st century. The depth information of the nonthermokarst lakes is retrieved directly from a 30 arc sec resolution Global Lake Database (GLDB) [Kourzeneva et al., 2012; Tan and Zhuang, 2015].

2.2. Simulation Protocol

We spin up the NHLEM model following the method of *van Huissteden et al.* [2011]. In the spin-up stage, the model is driven by an assumed climate change in 10,110 years starting from the level of the Last Glacial Termination (LGT) to the present time (2006). Specifically, for the first 100 years, air temperature and precipitation are set to increase gradually from the level of the LGT by 80% of the differences between the LGT and the present climate. For the next 1000 years, air temperature and precipitation are set to increase steadily to the present values. For the rest of the time, the present climate is used for the spin-up. During the spin-up, thaw lakes persisting for a long time are drained stochastically with the mean age of 3000 years [Brosius et al., 2012]. By the end of the spin-up, stable thaw lake extent is established. We then conduct two transient simulations for the variations of thaw lakes from 2006 to 2099 driven with an ensemble of climate change scenarios. It should be noted that as the permafrost extent has declined since the documentation of the circum-Arctic permafrost map in 2001 [Brown et al., 2002; Romanovsky et al., 2002], the present abundance of thermokarst lakes in the pan-Arctic could be overestimated slightly by the NHLEM model, e.g., in the south of the West Siberian Plain [Smith et al., 2005]. For the modeled thaw lakes, their water depth and talik thickness are updated yearly. To accelerate the bLake4Me model simulations, we adopt a tile scheme to construct a 0.5° × 0.5° resolution time-variant lake map from the simulated thaw lakes at less than 100 m resolutions. This tile scheme includes (1) identifying individual thaw lakes by detecting all connected lake pixels with the flood-fill connected-component labeling method [Meijster and Wilkinson, 2002], (2) classifying the lake pixels in each 0.5° × 0.5° grid into six groups (yedoma thaw lake margin, yedoma thaw lake center, nonyedoma thaw lake margin, nonyedoma thaw lake center, nonthaw lake margin, and nonthaw lake center) according to their ground ice and permafrost conditions, (3) calculating the shape factor of each lake by following the shape definition in *Ferland et al.* [2012] and assigning the value to all its pixels, and (4) congregating the lake pixels with comparable shape factors and depths in each group into a tile (or called cohort) with the *K*-means clustering method

[Seber, 1984]. Once the thaw lake map is made, combining the nonthaw lake map from GLDB, we then run the lake biogeochemical model in the same way as described by *Tan and Zhuang* [2015].

The past climate used in the spin-up is retrieved from a transient 21,000 year long ECBilt-CLIO Paleosimulation (SIM2b) which runs from 21,000 years before present into the preindustrial era [Timm and Timmermann, 2007; Timmermann et al., 2009]. The zonal and meridional spacing of climate fields in SIM2b are not homogeneous but close to 4.5°. To convert it to a finer 0.5° × 0.5° resolution for the use of the NHLEM model, we apply the delta-ratio bias correction method based on the observed half-degree 1900s climatology data from the Climate Research Unit (CRU2.0) and the thin-plate spline interpolation method, which is similar to the approach taken by *Hay et al.* [2000] to downscale and bias correct future climate scenarios. The future climate change in this study is synthesized from the Coupled Model Intercomparison Projection Phase 5 (CMIP5) RCP 2.6 (mild global warming) and RCP 8.5 (severe global warming) scenarios (Table S1) [Taylor et al., 2012]. The CMIP5 climate scenarios are downscaled with the inverse-square distance interpolation method and corrected with the delta-ratio bias correction method.

In the NHLEM model, the coefficients of thaw lake expansion to temperature and precipitation change are calculated according to the observations of *Jones et al.* [2011] at the northern Seward Peninsula, Alaska. During the period of 1973–1998, *Smith et al.* [2005] observed two contrasting trends of lake abundance and area in a Siberian permafrost zone: the total lake area increased by 12% in the continuous permafrost zone and declined by 13%, 12%, and 11% in the discontinuous, sporadic, and isolated permafrost zones, respectively. The initiation rates of thaw lakes are calibrated by minimizing the deviation of the simulated lake changes to this observation. Any other parameters used in the NHLEM model are kept consistent with the definitions of *van Huissteden et al.* [2011]. Using the computationally efficient tile scheme, it is possible to quantify the uncertainty of the modeled CH₄ emissions by running the bLake4Me model dozens of times with different sets of parameters sampled in line with their probability distribution functions (pdfs). The pdfs of the model's key parameters are evaluated with a Bayesian recursive parameter estimation method [Thiemann et al., 2001; Tang and Zhuang, 2009]. Based on a parameter sensitivity experiment [Tan et al., 2015], we conduct the uncertainty analysis for five key parameters including the carbon conversion rates of ¹⁴C-enriched and ¹⁴C-depleted carbon pools, the ¹⁴C-enriched carbon pool's Q₁₀ factor by which the methanogenic rate increases with a 10°C rise in temperature, the thermokarst margin erosion factor, and the critical damping depth of ¹⁴C-enriched carbon density.

3. Results and Discussion

3.1. Thaw Lake Dynamics

For evaluation, we first run the NHLEM model over the Kytalyk-Indigirka lowlands, Siberia, driven with map-derived environment conditions. This lowland region has been tested by *van Huissteden et al.* [2011] with their site level landscape evolution model. Our modeled area fraction of thaw lakes in the lowlands is 8.4% in 2006, close to their investigation of 8%. As shown in Figure S2, the NHLEM model estimates that thaw lakes in small sizes (less than 0.01 km²) have the highest fraction, similar to the work of *van Huissteden et al.* [2011]. But in contrast to the monotonic decrease of the modeled thaw lake area with lake size [van Huissteden et al., 2011], our test indicates that there is a high fraction of thaw lakes in sizes larger than 1 km². It should be noted that as limited by the resolution of the auxiliary maps, our tested region is not as homogeneous as the 400 km² lowlands investigated by *van Huissteden et al.* [2011]. Because it is almost 3 times larger in size and includes a higher fraction of highlands and a lower fraction of rivers and streams, the development of large thaw lakes could be favored. Similar to *van Huissteden et al.* [2011], our test predicts that the thawed area will increase, mainly as a result of lake expansion, to over 25% of the lowlands in the 2050s and thereafter decline as a result of lake drainage to nearly the initial level in the 2090s.

The NHLEM model is further tested in four Arctic regions much larger than the Kytalyk-Indigirka lowlands, including the Beaufort Coastal Plain in Alaska (160°W–144°W, 72°N–69°N), the Seward Peninsula (170°W–160°W, 67°N–64°N), Banks Island in Canada (127°W–120°W, 75°N–71°N), and the Indigirka-Kolyma lowlands in Russia (140°E–160°E, 73°N–68°N). The Seward Peninsula is underlain by discontinuous permafrost, while the other three regions are underlain by continuous permafrost. As these regions have been reported with intense thermokarst activities, we expect that the area of the modeled thaw lakes should be close to the lake area identified by GLWD. As expected, the difference between the simulated and mapped lake area is small in the Beaufort Coastal Plain (5544.5 km² versus 5961.8 km²) and the Indigirka-Kolyma lowlands (25,817.3 km²

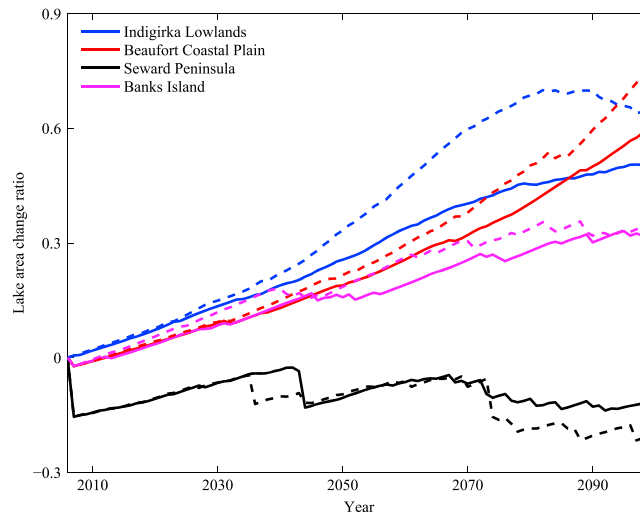


Figure 1. Change ratios of thaw lake areas in the four Arctic regions under two CMIP5 RCP climate scenarios. Solid lines represent the RCP 2.6 simulations, and dashed lines represent the RCP 8.5 simulations. The ratio is the relative increase or decrease of lake areas compared to the lake areas in 2006.

very likely that many small rivers and streams that are much thinner than 1 km, but important for thermokarst lake drainage, have been poorly represented in the map.

As shown in Figure 1, the area fraction of thaw lakes within those continuous permafrost zones is likely to increase during the 21st century, which is consistent with the field observations in the past decades [Smith et al., 2005; Kirpotin et al., 2008]. The lake abundance at the Seward Peninsula is projected to decline by 12% under RCP 2.6 and 20% under RCP 8.5. Due to its relatively higher annual temperature, this area will become unfavorable for the epigenetic ice reworking in drained basins [van Huissteden et al., 2011]. This projected decline is consistent with the report of a long-term investigation on the lake coverage of the peninsula's northern lowlands [Jones et al., 2011]. As indicated by Jones et al. [2011], from 1950 to 2007 the lake area on the lowlands had decreased by 14.9%. Overall, this evaluation indicates that the NHLEM model is robust in simulating the

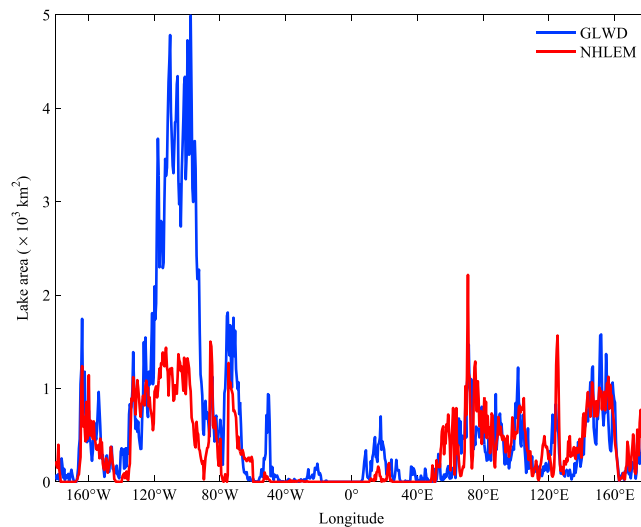


Figure 2. Zonal distribution of the modeled present-day thaw lakes as compared with the mapped lakes underlain by permafrost north of 60°N at a 0.5° resolution. The mapped lakes are retrieved from GLWD.

present-day and future abundance of thermokarst lakes in different pan-Arctic regions under complex environmental conditions and at the spatial scales much larger than the study of van Huissteden et al. [2011].

Figure 2 shows the comparison of the modeled and the mapped present-day lakes at the pan-Arctic scale. Apparently, the zonal distribution of pan-Arctic lakes in the NHLEM model and the GLWD database is consistent. For instance, the difference of the modeled and the mapped lake area in Siberia is small, agreeing with a claim that most of lakes in the Siberian permafrost zone are thermokarst lakes [Walter et al., 2006]. As GLWD only includes lakes much larger than 0.1 km² in size, the mapped lake area could be underestimated. To

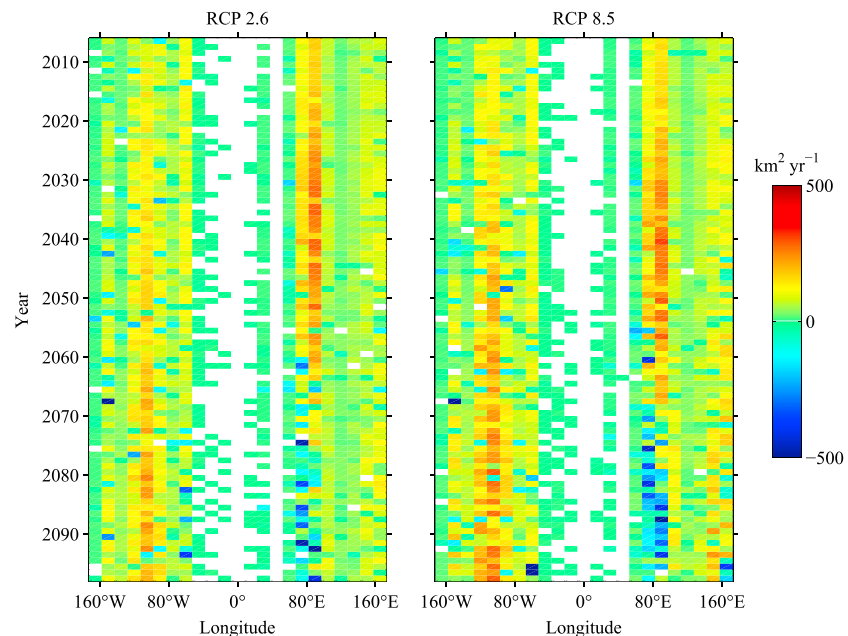


Figure 3. Hovmöller diagrams showing the annual zonal evolution of thaw lake areas in the pan-Arctic under two CMIP5 RCP climate scenarios at a 15° resolution.

correct it, we use a lake abundance-size statistical relationship [Verpoorter *et al.*, 2014] to include lakes smaller than 0.1 km². After the correction, we estimate that the total area of Russian lakes north of 60°N could be as large as 11.9×10^4 km². It means that the simulated thermokarst lakes (10.614×10^4 km²) comprise 89% of lakes in northern Russia, which is close to the estimate (90%) of Walter *et al.* [2006]. As expected, in northern Canada where the majority of lakes were formed by glacial activities [Wetzel, 2001], the modeled thaw lake area is much lower than the lake area identified by GLWD (Figure 2). Our simulated thaw lake area also agrees well with the estimates of the earlier investigations at the pan-Arctic and the Beringian scales. In the pan-Arctic, we estimate that the total area of thermokarst lakes is 25.949×10^4 km², which falls in the estimated range (25×10^4 – 38×10^4 km²) of Grosse *et al.* [2013a] over thermokarst lakes within the circum-Arctic permafrost zone with high to medium ground ice content. The total area of the modeled thermokarst lakes in Beringia is 10×10^4 km², which also falls in the estimated range (7.5×10^4 – 11.4×10^4 km²) of Brosius *et al.* [2012]. We estimate that the area ratio of Beringian thaw lakes to pan-Arctic thaw lakes is 38%, larger than the estimated ratio (30%) of Brosius *et al.* [2012]. This difference could be mainly caused by our underestimation of thermokarst lakes in northern Canada. In the NHLEM model, the Hudson Bay lowlands in northern Canada are identified as a region with low to medium ground ice content and thus are not favorable for thermokarst lakes [McGuire, 2013]. But this setting contradicts the investigation of Bouchard *et al.* [2014] in which a large number of thermokarst lakes were discovered in the lowlands. A possible reason is that the circum-Arctic ground ice map used in our study is not fine enough to resolve the small-scale permafrost with high ice content. Overall, this comparison implies that permafrost and topography conditions are the effective controls for the development of the pan-Arctic thermokarst landscape.

The variation of thaw lake abundance under global warming differs remarkably in the zonal direction, shown in Figure 3. Different from Smith *et al.* [2005, 2007], our simulations indicate that the extent of thaw lakes in the pan-Arctic will expand during the 21st century in most regions and the total area of thaw lakes will rise by 32.6% (or 8.464×10^4 km²) under RCP 2.6 and by 35.4% (or 9.174×10^4 km²) under RCP 8.5. This discrepancy could be mainly explained by the spatial gradient of annual mean air temperature in the pan-Arctic. For most of coastal lowlands along the Arctic Ocean, e.g., the Indigirka-Kolyma lowlands, air temperature remains low enough in the climate scenarios to sustain the refreezing of drained lake basins. In contrast, the West Siberian Plain, a region where Smith *et al.* [2005] observed the decline of thaw lakes, is relatively warm. Consequently, the lowlands have unfavorable conditions for the initiation and expansion of thermokarst lakes [van Huissteden *et al.*, 2011]. Our explanation is also consistent with the observation of Smith *et al.* [2005] over

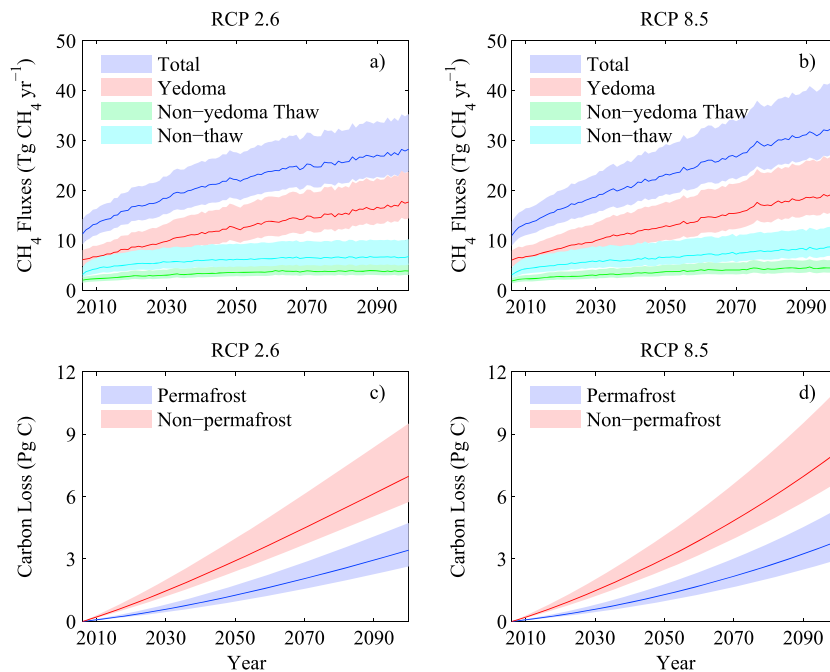


Figure 4. The projected annual CH₄ emissions from all Arctic lakes, all yedoma thaw lakes, and all nonyedoma lakes (nonyedoma thaw lakes and nonthaw lakes) and the projected cumulative amount of the permafrost and nonpermafrost carbon mineralization via methanogenesis in the pan-Arctic during the 21st century (shaded areas represent the 95% percentile confidence region of projections). (a) The projected annual CH₄ emissions under CMIP5 RCP 2.6, (b) the projected annual CH₄ emissions under CMIP5 RCP 8.5, (c) the projected cumulative carbon mineralization under CMIP5 RCP 2.6, and (d) the projected cumulative carbon mineralization under CMIP5 RCP 8.5.

the north of the West Siberian Plain. This continuous permafrost zone was observed to undergo the increase of lake abundance in the past decades. Since ice-rich lowlands are more extensive within continuous permafrost zones (Figure S1) [Brown *et al.*, 2002] and the continuous permafrost of the Arctic is unlikely to thaw out before 2100 [Koven *et al.*, 2015], our projections that the total area of pan-Arctic thaw lakes will increase during the 21st century are possible. The NHLEM model predicts that there are two zonal regions with a declining trend of thaw lakes from 2006 to 2099: southern Greenland (~ -24.5%) and European Russia (~ -7.2%). It should be noted that the simulated decline of thaw lakes in southern Greenland could be an overestimate because our model has not accounted for the initiation of thaw lakes at the retreating areas of the ice sheets. There are several zonal regions where the abundance of thaw lakes peaks in the middle of the 21st century, i.e., in the 2060s between 165°W and 150°W, about 2073 between 75°W and 60°W, about 2059 between 0° and 30°E, and about 2075 between 60°E and 90°E. The area of thaw lakes between 150°E and 180°E peaks in the 1980s under RCP 8.5 but rises steadily under RCP 2.6 during the 21st century. As illustrated before, the mechanisms that account for the stabilization of thaw lakes in those areas include the relatively high air temperature and the bounding of lake expansion by drained systems and highlands.

3.2. Impacts on Methane and Carbon Cycles

By incorporating the effects of both lake sediments warming and lake expansion, we estimate that CH₄ emissions from pan-Arctic lakes will increase from $11.3 \pm 2.1 \text{ Tg CH}_4 \text{ yr}^{-1}$ to $28.3 \pm 4.5 \text{ Tg CH}_4 \text{ yr}^{-1}$ (RCP 2.6) and $32.7 \pm 5.2 \text{ Tg CH}_4 \text{ yr}^{-1}$ (RCP 8.5), respectively (Figure 4). Specifically, the most striking rise is from the yedoma lakes, where the CH₄ emissions increase from $6.1 \pm 1.3 \text{ Tg CH}_4 \text{ yr}^{-1}$ to $17.7 \pm 3.3 \text{ Tg CH}_4 \text{ yr}^{-1}$ (RCP 2.6) and $19.6 \pm 3.6 \text{ Tg CH}_4 \text{ yr}^{-1}$ (RCP 8.5), respectively. CH₄ emissions from the nonthaw lakes will rise from $3.2 \pm 0.6 \text{ Tg CH}_4 \text{ yr}^{-1}$ to $6.8 \pm 1.6 \text{ Tg CH}_4 \text{ yr}^{-1}$ (RCP 2.6) and $8.7 \pm 1.8 \text{ Tg CH}_4 \text{ yr}^{-1}$ (RCP 8.5), respectively. The rising of CH₄ emissions from the nonyedoma thaw lakes is the mildest, which is from $2.0 \pm 0.5 \text{ Tg CH}_4 \text{ yr}^{-1}$ to $3.8 \pm 0.8 \text{ Tg CH}_4 \text{ yr}^{-1}$ (RCP 2.6) and $4.4 \pm 0.9 \text{ Tg CH}_4 \text{ yr}^{-1}$ (RCP 8.5), respectively. To evaluate the individual influence of lake evolution on the CH₄ emissions, we partition the increase of the lake CH₄ emissions into two parts: the increase from the lakes persisting from 2006 to 2099 and the increase from the newly formed

thermokarst lakes. The first part increase is driven by the warming of lake sediments, and the second part is driven by lake evolution. On average, 68% of the emission increase is caused by the warming of lake sediments and only 32% is caused by the initiation and expansion of thermokarst lakes. When assuming 1 ppb equivalent to 2.75 Tg CH₄ in the entire atmosphere [Khalil *et al.*, 2007] and the lifetime of atmospheric CH₄ as 8.9 years [Prinn *et al.*, 1995], we infer that approximately 55.0 to 69.3 ppb atmospheric CH₄ will be added, contributing a 0.02 to 0.026 W m⁻² increase of radiative forcing [Denman *et al.*, 2007]. Our simulated total CH₄ emissions (11.3 ± 2.1 Tg CH₄ yr⁻¹) from pan-Arctic lakes in 2006 fall in the estimated range (7.1–17.3 Tg CH₄ yr⁻¹) of Bastviken *et al.* [2011] and are only slightly lower than our previous estimate of 11.86 Tg CH₄ yr⁻¹ using a static lake map [Tan and Zhuang, 2015].

To evaluate to what extent the thermokarst lakes will disturb the Arctic permafrost carbon, we calculated the amount of the mineralized carbon that is mobilized from the thawing permafrost in the lake taliks. From 2006 to 2099, the projected loss of permafrost carbon via methanogenic mineralization is as large as 3.4 ± 0.8 Pg C under RCP 2.6 (Figure 4c) and 3.9 ± 0.9 Pg C under RCP 8.5 (Figure 4d). In contrast, a much larger amount (7.0 ± 1.9 Pg C under RCP 2.6 and 8.2 ± 2.2 Pg C under RCP 8.5) of the carbon mineralized by methanogens has nonpermafrost origins, e.g., transported from the active layers of lake catchments or fixed by lake vegetation. Relative to the sequestered permafrost organic carbon (about 1466 Pg) [Tarnocai *et al.*, 2009], the calculated carbon loss is small. The estimated carbon loss here is similar to the projections of Schuur *et al.* [2013] that range from 2.76 to 4.49 Pg C under RCP 8.5 and from 0.92 to 1.50 Pg C under RCP 2.6. Recently, several studies assessed the total permafrost carbon loss through both aerobic and anaerobic decompositions under global warming conditions. For instance, Schuur *et al.* [2015] estimated that the potential carbon release from the northern high-latitude permafrost zone by 2100 is in the range of 37–174 Pg C under RCP 8.5. If we assume 2.3% of the released permafrost carbon in the form of CH₄ [Schuur *et al.*, 2013] and a 1:1 ratio of anaerobic CH₄ to anaerobic CO₂ production [Walter Anthony *et al.*, 2014], the estimates of Schuur *et al.* [2015] correspond to that the permafrost carbon pool will be lost via methanogenesis by 1.8–8.0 Pg C, in the same magnitude as our estimates of 3.9 ± 0.9 Pg carbon loss.

As presented, the increase of CH₄ emissions from pan-Arctic lakes could be significant during the 21st century, on average, about 150% under RCP 2.6 and about 189% under RCP 8.5. There were few studies to directly evaluate the future CH₄ emissions from pan-Arctic lakes. From the earlier studies on boreal lakes and pan-Arctic wetlands, we conclude that the projected increase of the CH₄ emissions is likely because those ecosystems are similar to pan-Arctic lakes under warming conditions. For example, using soil incubations, Marotta *et al.* [2014] projected a 21–61% increase of CH₄ production in the anaerobic sediments of boreal lakes by the end of the 21st century under the Intergovernmental Panel on Climate Change B1 warming scenario. Because the Arctic could be warmed faster than the boreal regions [Kirtman *et al.*, 2013] and the methanogenesis of Arctic yedoma lakes could be fueled by the mobilization of labile Pleistocene age permafrost carbon [Walter *et al.*, 2006], the increase of CH₄ emissions from pan-Arctic lakes during the same period is higher. On average, our simulated increase is about 102% under RCP 2.6 and about 129% under RCP 8.5, respectively, when not considering the effect of thaw lake evolution. Further, if only the nonyedoma lakes are included, the increase is about 71% under RCP 2.6, close to the upper bound given by Marotta *et al.* [2014]. The expert assessment on the increase of CH₄ emissions from the thawing permafrost is as large as 20 Tg CH₄ yr⁻¹ under RCP 2.6 and 80 Tg CH₄ yr⁻¹ under RCP 8.5, respectively, [Schuur *et al.*, 2013]. If assuming that a half of this increase originated from lakes [Riley *et al.*, 2011; Tan and Zhuang, 2015], the lakes north of 60°N could contribute an increase of 10–40 Tg CH₄ yr⁻¹, a magnitude close to our estimates (17–21.4 Tg CH₄ yr⁻¹). Walter *et al.* [2007a] estimated that under warming conditions, the expansion of yedoma thermokarst lakes on the exposed yedoma surface alone, including the continental shelf currently inundated by the Arctic Ocean, could have released as much as 20–26 Tg CH₄ yr⁻¹ around 11.5 kyr B.P. This possible abrupt rise of CH₄ emissions from pan-Arctic lakes during the Holocene Thermal Maximum implies that our simulations should not be a surprise.

By using an Earth system model without the lake biogeochemistry and evolution processes, Gao *et al.* [2013] projected a very low increase of CH₄ emissions from the lakes north of 45°N by 2100, at 1.1–1.8 Tg CH₄ yr⁻¹ under low warming scenarios and 1.9–3.0 Tg CH₄ yr⁻¹ under high warming scenarios. Their study probably underestimated the future CH₄ emissions from northern high-latitude lakes. First, the modeled present-day CH₄ emissions from the lakes in Gao *et al.* [2013] are extremely low, only about 4 Tg CH₄ yr⁻¹, which is substantially lower than the estimate (larger than 14 Tg CH₄ yr⁻¹) of Bastviken *et al.* [2011]. Second, the

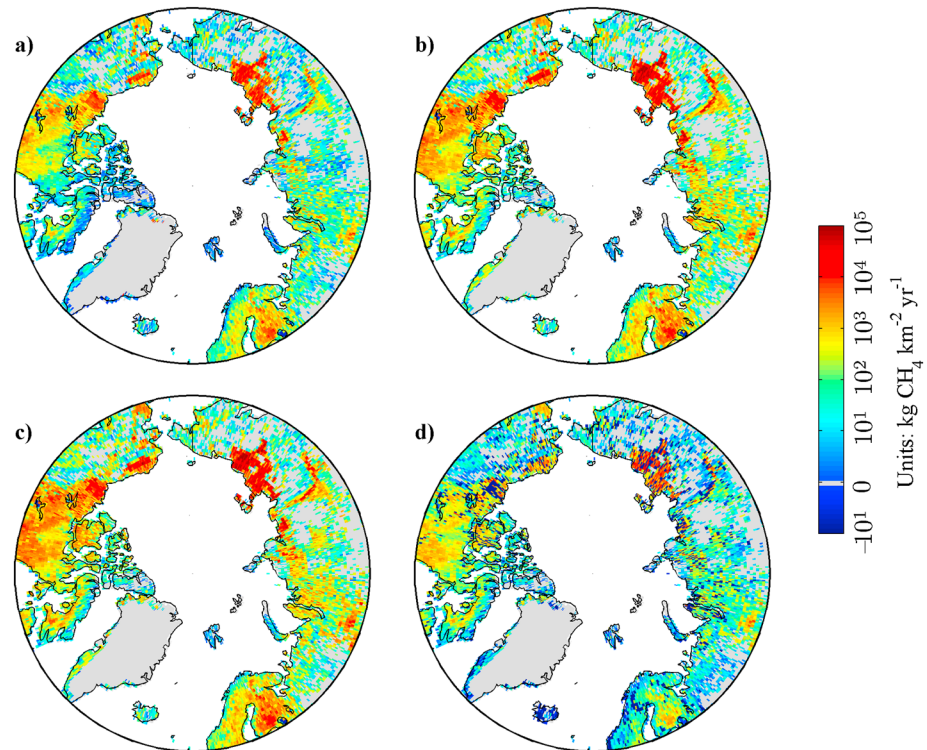


Figure 5. The projected evolution of CH₄ emissions from pan-Arctic lakes under the future climate scenarios: (a) the CH₄ emissions in 2006, (b) the CH₄ emissions in 2099 under CMIP5 RCP 2.6, (c) the CH₄ emissions in 2099 under CMIP5 RCP 8.5, and (d) the difference of the CH₄ emissions in 2099 between Figures 5c and 5b.

Q_{10} (3.0) of methanogenesis used in *Gao et al.* [2013] is lower than the Q_{10} (about 3.8) inferred from a recent global investigation [*Yvon-Durocher et al.*, 2014]. Third, the area of the high-flux yedoma lakes could be underestimated in *Gao et al.* [2013]. Their study used a fixed wetland/lake area ratio to infer lake abundance from inundation abundance, but the coastal lowlands of northeastern Siberia and northern Canada could have higher wetland/lake area ratios [*Paltan et al.*, 2015].

Spatially, the CH₄ flux hot spots, such as the Siberian coastal lowlands, could contribute more CH₄ emission increases than the regions with less CH₄ fluxes at present (e.g., from the interior Alaska) (Figure 5). The spatial variations of the lake CH₄ fluxes in the pan-Arctic are mainly controlled by topography and yedoma permafrost extent. Figure 5 also indicates that some permafrost-free areas with high abundance of low-flux lakes, e.g., Finland, can contribute significant amounts of CH₄ emissions. As shown in Figure 5d, while the warming in RCP 8.5 is much stronger, the regional CH₄ emissions under RCP 8.5 are not always larger than the emissions under RCP 2.6 in the pan-Arctic. This negative effect of air temperature on the CH₄ emissions can be explained by the evolution of thaw lakes. In a warmer climate, the drainage risk of thaw lakes in some regions can be raised by their fast expansion (Figures 1 and 3).

The modeled CH₄ emissions in 2006 and 2099 from the lakes of four major Arctic regions are presented in Table 1. The modeled CH₄ emissions are the largest in northern Siberia and northern Canada where a large number of thermokarst lakes are located. This finding is consistent with our previous work [*Tan and Zhuang*, 2015] and also supported by the studies of *Walter et al.* [2006] and *Laurion et al.* [2010]. But different from *Tan and Zhuang* [2015] in which the lakes in northern Siberia and northern Canada were estimated to contribute almost equally to the global CH₄ cycle (4.96 Tg CH₄ yr⁻¹ versus 5.02 Tg CH₄ yr⁻¹), this study estimates that CH₄ emissions from the lakes in northern Siberia are much larger. This difference is caused by the better representation of thermokarst lakes in northern Canada using the NHLEM model. In addition, thanks to its high resolution, the NHLEM model can estimate the distribution of small size yedoma lakes (<0.1 km²) in Siberia that are indiscernible in the 1 km resolution GLDB lake map used in *Tan and Zhuang* [2015].

Table 1. Modeled Regional CH₄ Emissions (Tg CH₄ yr⁻¹) From the Lakes North of 60°N Under the Present Boundary Conditions and Two Future Climate Scenarios^a

Name	Present	RCP 2.6	RCP 8.5
Alaska	1.0 ± 0.2	2.4 ± 0.4	2.8 ± 0.5
Northern Canada	2.6 ± 0.4	5.8 ± 0.8	7.4 ± 1.0
Northern Europe	1.2 ± 0.2	2.2 ± 0.5	2.4 ± 0.4
Northern Siberia	6.4 ± 1.4	17.7 ± 3.2	19.9 ± 3.6

^aThe ± sign means standard deviation of CH₄ emissions.

Because the thermokarst margins of the small size yedoma lakes are CH₄ flux hot spots [Walter *et al.*, 2006], it is very likely that the lake CH₄ emissions in northern Siberia were underestimated in Tan and Zhuang [2015]. As presented in Table 1 and Figure 5c, with the thawing of the carbon-rich yedoma permafrost, the lakes in Siberia are predicted to contribute the largest CH₄ emission increase [Walter *et al.*, 2006]. The increase of CH₄ emissions from Canadian lakes (Table 1 and Figure 5c) is also prominent, which is driven by both the mineralization of yedoma permafrost carbon at the delta of Mackenzie River [Brosius *et al.*, 2012] and the high lake abundance in the Canadian Shield [Wetzel, 2001; Lehner and Döll, 2004].

As shown in Figure 6, the change of CH₄ emissions from pan-Arctic lakes varies seasonally. When comparing the simulated monthly average CH₄ emissions between the period of 2006–2009 and the period of 2096–2099, we find that the CH₄ emissions are boosted relatively more in cold months than in warm months. This is because with the warming of the Arctic, lake ice and snow covers will form later and melt earlier, and a large amount of CH₄ that previously could be oxidized or blocked by ice and snow is now able to release in spring and late fall [Karlsson *et al.*, 2013; Greene *et al.*, 2014]. Figure 6 shows that in June and July, the total CH₄ emissions under RCP 2.6 even exceed the emissions under RCP 8.5. This phenomenon is probably caused by the out-of-sync breaking time of the lake ice covers under the two climate scenarios. Pan-Arctic lakes are projected to lose their ice covers in June and July under RCP 2.6 and in April and May under RCP 8.5 in the 2090s, respectively. As a result, the large release of the CH₄ accumulated under winter ice covers will occur in early summer under RCP 2.6 rather than in late spring under RCP 8.5.

4. Limitations of the Study and Future Work

Our model simulations suggest that by the end of the 21st century CH₄ emissions from pan-Arctic lakes could be as large as nearly 3 times the present-day values and close to the current CH₄ emissions from the northern high-latitude wetlands [Zhuang *et al.*, 2004]. Although the warming of permafrost could threaten the develop-

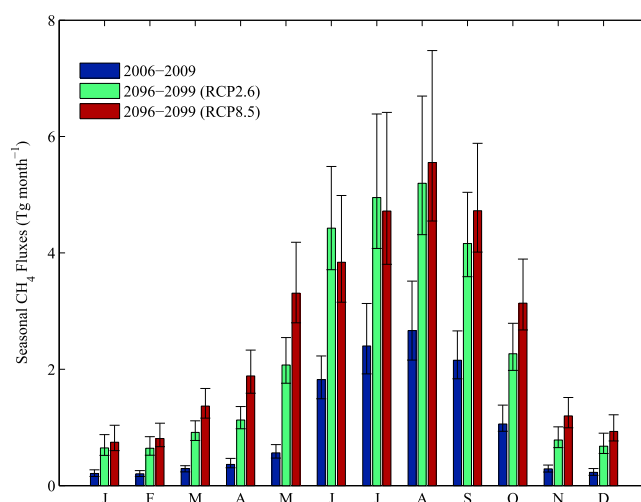


Figure 6. Seasonal variations of CH₄ emissions from pan-Arctic lakes in the period of 2006–2009 and the period of 2096–2099.

ment of thermokarst lakes, the stronger control of sediments temperature on CH₄ emissions indicated by this study implies that the growth of this source could be sustained even after 2100. However, it is still uncertain whether the emissions can increase to as large as 50–100 Tg CH₄ yr⁻¹, as suggested by Walter *et al.* [2007b]. In our study, the nonpermafrost carbon pool is fixed during the simulations. But due to the terrestrialization process, this carbon pool should be variable [Walter Anthony *et al.*, 2014]. Thus, to properly quantify the carbon dynamics in pan-Arctic lakes, it is important to incorporate the cycling of dissolved organic carbon, particulate organic carbon, and dissolved inorganic carbon into

the lake biogeochemical model. Another weakness of the method is that few observations from the nonthaw lakes in the pan-Arctic have been used to constrain the lake biogeochemical model [Tan *et al.*, 2015], which could bias our estimation of CH₄ emissions from the nonthaw lakes.

There are also some weaknesses in our landscape evolution model that could limit the accuracy of the simulations. First, the NHLEM model is not fully process based. For instance, the influence of ground water to lake evolution in the permafrost zone has not been integrated. As pointed out by the earlier studies, after permafrost thaws, the impact of ground water on the hydrology of thaw lakes could become substantial [Yoshikawa and Hinzman, 2003; Wellman *et al.*, 2013]. Second, our assumption that thermokarst lakes can only develop in non-sandy, ice-rich lowland permafrost zones could be too stringent because Hinkel *et al.* [2012] observed that in Alaska thaw lakes can exist in areas underlain by sandy ground. Third, our assumption that the abundance of the nonthaw lakes is kept constant throughout the 21st century is probably unrealistic. As described by Smith *et al.* [2007], during the ground transition from a permafrost zone to a permafrost-free zone, thaw lakes could be substituted by nonthaw lakes and nonthaw lakes could be changed by hydrological processes. Fourth, as illustrated, the estimates of the thaw lake extent can be refined by using finer-resolution geospatial data sets of topography, ground ice content, and river networks. In spite of these limitations, our simulations of the expansion and drainage of thermokarst lakes suggest that some algorithms in the NHLEM model can be used in more complex lake evolution models, including the control of lake evolution by topography, ground ice, and drainage networks, and the stochastic initiation of thermokarst depressions [Harris, 2002; Bouchard *et al.*, 2014].

Acknowledgments

The authors appreciate the insightful comments from two anonymous reviewers. We acknowledge the World Climate Research Programme's Working Group on Coupled Modeling, which is responsible for CMIP, for producing and making available their model output. For CMIP, the U.S. Department of Energy's Program for Climate Model Diagnosis and Intercomparison provides coordinating support and led development of software infrastructure in partnership with the Global Organization for Earth System Science Portals. GTOPO30 and HYDRO1K products are available from the U.S. Geological Survey. This study is supported through projects funded to Q.Z. by the NASA Land Use and Land Cover Change program (NASA-NNX09AI26G), Department of Energy (DE-FG02-08ER64599), the NSF Division of Information and Intelligent Systems (NSF-1028291), and the NSF Carbon and Water in the Earth Program (NSF-0630319). This research is also in part supported by the Director, Office of Science, Office of Biological and Environmental Research of the U.S. Department of Energy under contract DE-AC02-05CH11231 as part of their Earth System Modeling Program. The supercomputing resource is provided by Rosen Center for Advanced Computing at Purdue University. All data presented in this paper are publicly accessible: ECBilt-CLIO Paleosimulation (<http://apdrc.soest.hawaii.edu/datadoc/sim2bl.php>), CRU2.0 (<http://www.cru.uea.ac.uk/data>), CMIP5 RCP 2.6 and RCP 8.5 climate scenarios (<http://pcmdi9.llnl.gov/esgf-web-fe/>), Circum-Arctic Map of Permafrost and Ground Ice Conditions database (<http://insidc.org/data/ggd318>), USGS GTOPO30 (<ftp://edcftp.cr.usgs.gov/data/gtopo30/>), USGS HYDRO1K (<ftp://edcftp.cr.usgs.gov/data/gtopo30hydro/>), Harmonized World Soil Database version 1.2 (<http://webarchive.iiasa.ac.at/Research/LUC/External-World-soil-database/HTML/>), Global Lakes and Wetlands Database (<https://www.worldwildlife.org/pages/global-lakes-and-wetlands-database>), and Late Pleistocene Ice-Rich Syngenetic Permafrost of the Yedoma Suite in East and Central Siberia and North America (<http://pubs.usgs.gov/of/2013/1078/> and <http://geogratis.gc.ca/api/en/nrcan-rcan/ess-sst/146c4b1f-52b9-5589-a919-c150d1558a03.html>).

5. Conclusion

By coupling the projected thaw lake extent from a landscape evolution model with a lake biogeochemical model, we estimate that by 2100, CH₄ emissions from pan-Arctic lakes will be 28.3 ± 4.5 Tg CH₄ yr⁻¹ under a low warming scenario and 32.7 ± 5.2 Tg CH₄ yr⁻¹ under a high warming scenario, which are about 2.5 and 2.9 times the present-day emissions. Our models estimate that methanogens will mineralize 3.4 ± 0.8 Pg C (under RCP 2.6) and 3.9 ± 0.9 Pg C (under RCP 8.5) of the permafrost carbon from 2006 to 2099. Although the mineralized permafrost carbon only represents a small fraction of the global permafrost carbon pool, the projected CH₄ emissions will increase atmospheric CH₄ concentrations by almost 4%, exerting 0.02 to 0.026 W m⁻² extra radiative forcing to the atmosphere. The mineralized carbon with nonpermafrost origins is 7.0 ± 1.9 Pg C under RCP 2.6 and 8.2 ± 2.2 Pg C under RCP 8.5, respectively. Spatially, the regions with high lake area fractions or extensive yedoma lakes will contribute more CH₄ emission increases in the future. Seasonally, as global warming will shorten the duration of lake ice covers, the CH₄ emissions in April and May will rise substantially. Our study indicates that the increase of lake sediments' temperature is the dominant factor to drive CH₄ emissions from pan-Arctic lakes during the 21st century.

References

- Allard, M., S. Caron, and Y. Begin (1996), Climatic and ecological controls on ice segregation and thermokarst: The case history of a permafrost plateau in northern Quebec, *Permafrost Periglacial Process.*, *7*, 207–227.
- Andreae, M. O., and P. Merlet (2001), Emission of trace gases and aerosols from biomass burning, *Global Biogeochem. Cycles*, *15*, 955–966, doi:10.1029/2000GB001382.
- Avis, C. A., A. J. Weaver, and K. J. Meissner (2011), Reduction in areal extent of high-latitude wetlands in response to permafrost thaw, *Nat. Geosci.*, *4*, 444–448, doi:10.1038/ngeo1160.
- Bastviken, D., J. Cole, M. Pace, and L. Tranvik (2004), Methane emissions from lakes: Dependence of lake characteristics, two regional assessments, and a global estimate, *Global Biogeochem. Cycles*, *18*, GB4009, doi:10.1029/2004GB002238.
- Bastviken, D., L. Tranvik, J. Downing, P. M. Crill, and A. Enrich-Prast (2011), Freshwater methane emissions offset the continental carbon sink, *Science*, *331*, 50–50.
- Bouchard, F., P. Francus, R. Pienitz, I. Laurion, and S. Fyfe (2014), Subarctic thermokarst ponds: Investigating recent landscape evolution and sediment dynamics in thawed permafrost of Northern Québec (Canada), *Arctic, Antarct. Alp. Res.*, *46*, 251–271.
- Brosius, L. S., K. M. Walter Anthony, G. Grosse, J. P. Chanton, L. M. Farquharson, P. Overduin, and H. Meyer (2012), Using the deuterium isotope composition of permafrost meltwater to constrain thermokarst lake contributions to atmospheric CH₄ during the last deglaciation, *J. Geophys. Res.*, *117*, G01022, doi:10.1029/2011JG001810.
- Brown, J., O. J. Ferrians, J. A. Heginbottom, and E. S. Melnikov (2002), *Circum-Arctic Map of Permafrost and Ground-Ice Conditions, Version 2*, Natl. Snow and Ice Data Center, Boulder, Colo.
- Campeau, A., J. Lapierre, D. Vachon, and P. del Giorgio (2014), Regional contribution of CO₂ and CH₄ fluxes from the fluvial network in a lowland boreal landscape of Québec, *Global Biogeochem. Cycles*, *28*, 57–69, doi:10.1002/2013GB004685.
- Chen, M., J. C. Rowland, C. J. Wilson, G. L. Altmann, and S. P. Brumby (2013), The importance of natural variability in lake areas on the detection of permafrost degradation: A case study in the Yukon Flats, Alaska, *Permafrost Periglacial Process.*, *24*, 224–240.

- Denman, K. L., et al. (2007), Couplings between changes in the climate system and biogeochemistry, in *Climate Change 2007: The Physical Science Basis. Contribution of Working Group I to the Fourth Assessment Report of the Intergovernmental Panel on Climate Change*, edited by S. Solomon et al., chap. 7, pp. 501–587, Cambridge Univ. Press, Cambridge, U. K.
- Dragokoenky, E. J., E. G. Nisbet, R. Fisher, and D. Lowry (2011), Global atmospheric methane: Budget, changes and dangers, *Philos. Trans. R. Soc., A*, *369*, 2058–2072.
- Everett, K. R. (1980), Landforms, in *Geobotanical Atlas of the Prudhoe Bay Region, Alaska*, edited by D. A. Walker et al., Rep. 80–14, pp. 14–19, U.S. Army Cold Regions Res. and Eng. Lab., Hanover, N. H.
- FAO/IIASA/ISRIC/ISSCAS/JRC (2012), *Harmonized World Soil Database, Version 1.2*, FAO and IIASA, Rome, Italy and Laxenburg, Austria.
- Ferland, M.-E., P. A. del Giorgio, C. R. Teodoru, and Y. T. Prairie (2012), Long-term C accumulation and total C stocks in boreal lakes in northern Québec, *Global Biogeochem. Cycles*, *26*, GB0E04, doi:10.1029/2011GB004241.
- Gao, X., C. Adam Schlosser, A. Sokolov, K. Walter Anthony, Q. Zhuang, and D. Kicklighter (2013), Permafrost degradation and methane: Low risk of biogeochemical climate-warming feedback, *Environ. Res. Lett.*, *8*, 035014, doi:10.1088/1748-9326/8/3/035014.
- Greene, S., K. M. Walter Anthony, D. Archer, A. Sepulveda-Jauregui, and K. Martinez-Cruz (2014), Modeling the impediment of methane ebullition bubbles by seasonal lake ice, *Biogeosciences*, *11*, 6791–6811, doi:10.5194/bg-11-6791-2014.
- Grosse, G., G. M. Jones, and C. D. Arp (2013a), Thermokarst lakes, drainage, and drained basins, in *Treatise on Geomorphology 8*, edited by J. F. Shroder Jr., pp. 325–353, Elsevier, Amsterdam, Netherlands.
- Grosse, G., J. E. Robinson, R. Bryant, M. D. Taylor, W. Harper, A. DeMasi, E. Kyker-Snowman, A. Veremeeva, L. Schirrmeister, and J. Harden (2013b), Distribution of late Pleistocene ice-rich syngenetic permafrost of the Yedoma Suite in east and central Siberia, Russia, U.S. Geological Survey Open File Report 2013–1078, 37 p.
- Harris, S. A. (2002), Causes and consequences of rapid thermokarst development in permafrost or glacial terrain, *Permafrost Periglacial Process.*, *13*, 237–242.
- Hay, L. E., R. L. Wilby, and G. H. Leavesley (2000), A comparison of delta change and downscaled GCM scenarios for three mountainous basins in the United States, *J. Am. Water Resour. Assoc.*, *36*, 387–397.
- Hinkel, K. M., Y. Sheng, J. D. Lenters, E. A. Lyons, R. A. Beck, W. R. Eisner, and J. Wang (2012), Thermokarst lakes on the arctic coastal plain of Alaska: Geomorphic controls on bathymetry, *Permafrost Periglacial Process.*, *23*, 218–230, doi:10.1002/ppp.1744.
- Jones, B. M., G. Grosse, C. D. Arp, M. C. Jones, K. M. Walter Anthony, and V. E. Romanovsky (2011), Modern thermokarst lake dynamics in the continuous permafrost zone, northern Seward Peninsula, Alaska, *J. Geophys. Res.*, *116*, G00M03, doi:10.1029/2011JG001666.
- Jorgenson, M. T., and Y. Shur (2007), Evolution of lakes and basins in northern Alaska and discussion of the thaw lake cycle, *J. Geophys. Res.*, *112*, F02S17, doi:10.1029/2006JF000531.
- Karlsson, J., R. Giesler, J. Persson, and E. Lundin (2013), High emission of carbon dioxide and methane during ice thaw in high latitude lakes, *Geophys. Res. Lett.*, *40*, 1123–1127, doi:10.1002/grl.501.
- Khalil, M. A. K., C. L. Butenhoff, and R. A. Rasmussen (2007), Atmospheric methane: Trends and cycles of sources and sinks, *Environ. Sci. Technol.*, *41*, 2131–2137.
- Kirpotin, S., Y. Polishchuk, E. Zakharova, L. Shirokova, O. Pokrovsky, M. Kolmakova, and B. Dupre (2008), One of the possible mechanisms of thermokarst lakes drainage in West-Siberian North, *Int. J. Environ. Stud.*, *65*, 631–635.
- Kirtman, B., et al. (2013), Near-term climate change: Projections and predictability, in *Climate Change 2013: The Physical Science Basis. Contribution of Working Group I to the Fifth Assessment Report of the Intergovernmental Panel on Climate Change*, edited by T. F. Stocker et al., Cambridge Univ. Press, Cambridge, U. K., and New York.
- Kourzeneva, E., H. Asensio, E. Martin, and S. Faroux (2012), Global gridded dataset of lake coverage and lake depth for use in numerical weather prediction and climate modelling, *Tellus A*, *64*, 1–14.
- Koven, C. D., D. M. Lawrence, and W. J. Riley (2015), Permafrost carbon-climate feedback is sensitive to deep soil carbon decomposability but not deep soil nitrogen dynamics, *Proc. Natl. Acad. Sci. U.S.A.*, *112*, 3752–3757, doi:10.1073/pnas.1415123112.
- Laurion, I., W. Vincent, S. MacIntyre, L. Retamal, C. Dupont, P. Francus, and R. Pienitz (2010), Variability in greenhouse gas emissions from permafrost thaw ponds, *Limnol. Oceanogr.*, *55*, 115–133, doi:10.4319/lo.2010.55.1.0115.
- Lee, H., S. C. Swenson, A. G. Slater, and D. M. Lawrence (2014), Effects of excess ground ice on projections of permafrost in a warming climate, *Environ. Res. Lett.*, *9*, 124006, doi:10.1088/1748-9326/9/12/124006.
- Lehner, B., and P. Döll (2004), Development and validation of a global database of lakes, reservoirs and wetlands, *J. Hydrol.*, *296*, 1–22.
- Louis, V., C. Kelly, É. Duchemin, J. Rudd, and D. Rosenberg (2000), Reservoir surfaces as sources of greenhouse gases to the atmosphere: A global estimate, *BioScience*, *50*, 766–775.
- Manasypov, R. M., et al. (2015), Seasonal dynamics of organic carbon and metals in thermokarst lakes from the discontinuous permafrost zone of western Siberia, *Biogeosciences*, *12*, 3009–3028, doi:10.5194/bg-12-3009-2015.
- Marotta, H., L. Pinho, C. Gudas, D. Bastviken, L. J. Tranvik, and A. Enrich-Prast (2014), Greenhouse gas production in low-latitude lake sediments responds strongly to warming, *Nat. Clim. Change*, *4*, 11–14, doi:10.1038/NCLIMATE2222.
- McGuire, A. D. (2013), Modeling thermokarst dynamics in boreal and Arctic regions of Alaska and Northwest Canada: A white paper, The Thermokarst Working Group of the Integrated Ecosystem Model for Alaska and Northwest Canada, 1–27.
- Meijster, A., and M. H. Wilkinson (2002), A comparison of algorithms for connected set openings and closings: Pattern analysis and machine intelligence, *IEEE Trans.*, *24*, 484–494.
- Myhre, G., et al. (2013), Anthropogenic and natural radiative forcing, in *Climate Change 2013: The Physical Science Basis. Contribution of Working Group I to the Fifth Assessment Report of the Intergovernmental Panel on Climate Change*, edited by T. F. Stocker et al., Cambridge Univ. Press, Cambridge, U. K., and New York.
- Paltan, H., J. Dash, and M. Edwards (2015), A refined mapping of Arctic lakes using Landsat imagery, *Int. J. Remote Sens.*, *36*, 5970–5982, doi:10.1080/01431161.2015.1110263.
- Prinn, R., R. Weiss, B. Miller, J. Huang, and F. Aleya (1995), Atmospheric trends and lifetime of CH₃CCl₃ and global OH concentrations, *Science*, *269*, 187–192.
- Riley, W. J., Z. M. Subin, D. M. Lawrence, S. C. Swenson, M. S. Torn, L. Meng, N. M. Mahowald, and P. Hess (2011), Barriers to predicting changes in global terrestrial methane fluxes: Analyses using CLM4Me, a methane biogeochemistry model integrated in CESM, *Biogeosciences*, *8*, 1925–1953, doi:10.5194/bg-8-1925-2011.
- Riordan, B., D. Verbyla, and A. D. McGuire (2006), Shrinking ponds in subarctic Alaska based on 1950–2002 remotely sensed images, *J. Geophys. Res.*, *111*, G04002, doi:10.1029/2005JG000150.
- Romanovsky, V. E., M. Burgess, S. Smith, K. Yoshikawa, and J. Brown (2002), Permafrost temperature records: Indicators of climate change, *Eos Trans. AGU*, *83*, 589, doi:10.1029/2002EO000402.

- Sawakuchi, H. O., D. Bastviken, A. O. Sawakuchi, A. V. Krusche, M. V. R. Ballester, and J. E. Richey (2014), Methane emissions from Amazonian Rivers and their contribution to the global methane budget, *Global Change Biol.*, *20*, 2829–2840, doi:10.1111/gcb.12646.
- Schuur, E. A. G., et al. (2013), Expert assessment of vulnerability of permafrost carbon to climate change, *Clim. Change*, *119*, 359–374, doi:10.1007/s10584-013-0730-7.
- Schuur, E. A. G., et al. (2015), Climate change and the permafrost carbon feedback, *Nature*, *520*, 171–179, doi:10.1038/nature14338.
- Seber, G. A. F. (1984), *Multivariate Observations*, John Wiley, Hoboken, N. J.
- Shirokova, L. S., O. S. Pokrovsky, S. N. Kirpotin, and B. Dupré (2009), Heterotrophic bacterio-plankton in thawed lakes of the northern part of Western Siberia controls the CO₂ flux to the atmosphere, *Int. J. Environ. Stud.*, *66*, 433–445, doi:10.1080/00207230902758071.
- Smith, L. G., Y. Sheng, G. M. MacDonald, and L. D. Hinzman (2005), Disappearing Arctic lakes, *Science*, *308*, 1429–1429.
- Smith, L. G., Y. Sheng, and G. M. MacDonald (2007), A first pan-Arctic assessment of the influence of glaciation, permafrost, topography and peatlands on northern hemisphere lake distribution, *Permafrost Periglacial Process.*, *208*, 201–208, doi:10.1002/ppp.581.
- Spencer, R. G. M., P. J. Mann, T. Dittmar, T. I. Eglinton, C. Mcintyre, R. M. Holmes, N. Zimov, and A. Stubbins (2015), Detecting the signature of permafrost thaw in Arctic rivers, *Geophys. Res. Lett.*, *42*, 2830–2835, doi:10.1002/2015GL063498.
- Tan, Z., and Q. Zhuang (2015), Arctic lakes are continuous methane sources to the atmosphere under warming conditions, *Environ. Res. Lett.*, *10*, 054016, doi:10.1088/1748-9326/10/5/054016.
- Tan, Z., Q. Zhuang, and K. M. Walter Anthony (2015), Modeling methane emissions from Arctic lakes: Model development and site-level study, *J. Adv. Model. Earth Syst.*, *7*, 459–483, doi:10.1002/2014MS000314.
- Tang, J., and Q. Zhuang (2009), A global sensitivity analysis and Bayesian inference framework for improving the parameter estimation and prediction of a process-based Terrestrial Ecosystem Model, *J. Geophys. Res.*, *114*, D15303, doi:10.1029/2009JD011724.
- Tarnocai, C., J. G. Canadell, E. A. G. Schuur, P. Kuhry, G. Mazhitova, and S. Zimov (2009), Soil organic carbon pools in the northern circumpolar permafrost region, *Global Biogeochem. Cycles*, *23*, GB2023, doi:10.1029/2008GB003327.
- Taylor, K. E., R. J. Stouffer, and G. A. Meehl (2012), An overview of CMIP5 and the experiment design, *Bull. Am. Meteorol. Soc.*, *93*, 485–498.
- Thiemann, M., M. Trosset, H. Gupta, and S. Sorooshian (2001), Bayesian recursive parameter estimation for hydrologic models, *Water Resour. Res.*, *37*, 2521–2535.
- Thornton, B. F., M. Wik, and P. M. Crill (2015), Climate-forced changes in available energy and methane bubbling from subarctic lakes, *Geophys. Res. Lett.*, *42*, 1936–1942, doi:10.1002/2015GL063189.
- Timm, O., and A. Timmermann (2007), Simulation of the last 21 000 years using accelerated transient boundary conditions, *J. Clim.*, *20*, 4377–4401.
- Timmermann, A., O. Timm, L. Stott, and L. Menviel (2009), The roles of CO₂ and orbital forcing in driving southern hemispheric temperature variations during the last 21 000 Yr*, *J. Clim.*, *22*, 1629–1640.
- van Huissteden, J., C. Berrittella, F. J. W. Parmentier, Y. Mi, T. C. Maximov, and A. J. Dolman (2011), Methane emissions from permafrost thaw lakes limited by lake drainage, *Nat. Clim. Change*, *1*, 119–123, doi:10.1038/nclimate1101.
- Verpoorter, C., T. Kutser, D. A. Seekell, and L. J. Tranvik (2014), A global inventory of lakes based on high-resolution satellite imagery, *Geophys. Res. Lett.*, *41*, 6396–6402, doi:10.1002/2014GL060641.
- Walter Anthony, K. M., et al. (2014), A shift of thermokarst lakes from carbon sources to sinks during the Holocene epoch, *Nature*, *511*, 452–456, doi:10.1038/nature13560.
- Walter, K. M., S. A. Zimov, J. P. Chanton, D. Verbyla, and F. S. Chapin III (2006), Methane bubbling from Siberian thaw lakes as a positive feedback to climate warming, *Nature*, *443*, 71–75, doi:10.1038/nature05040.
- Walter, K. M., M. E. Edwards, G. Grosse, S. A. Zimov, and F. S. Chapin III (2007a), Thermokarst lakes as a source of atmospheric CH₄ during the last deglaciation, *Science*, *318*, 633–636, doi:10.1126/science.1142924.
- Walter, K. M., L. C. Smith, and F. S. Chapin III (2007b), Methane bubbling from northern lakes: Present and future contributions to the global methane budget, *Philos. Trans. R. Soc., A*, *365*, 1657–1676, doi:10.1098/rsta.2007.2036.
- Walter, K. M., J. P. Chanton, F. S. Chapin III, E. A. G. Schuur, and S. A. Zimov (2008), Methane production and bubble emissions from arctic lakes: Isotopic implications for source pathways and ages, *J. Geophys. Res.*, *113*, G00A08, doi:10.1029/2007JG000569.
- Wellman, T. P., C. I. Voss, and M. A. Walvoord (2013), Impacts of climate, lake size, and supra- and sub-permafrost groundwater flow on lake-talik evolution, Yukon Flats, Alaska (USA), *Hydrogeol. J.*, *21*, 281–298.
- West, J. J., and L. J. Plug (2008), Time-dependent morphology of thaw lakes and taliks in deep and shallow ground ice, *J. Geophys. Res.*, *113*, F01009, doi:10.1029/2006JF000696.
- Wetzel, R. G. (2001), *Limnology: Lake and River Ecosystems*, chap. 3, pp. 26–30, Academic Press, San Diego, Calif.
- Wik, M., B. F. Thornton, D. Bastviken, S. MacIntyre, R. K. Varner, and P. M. Crill (2014), Energy input is primary controller of methane bubbling in subarctic lakes, *Geophys. Res. Lett.*, *41*, 555–560, doi:10.1002/2013GL058510.
- Wolfe, S. A., A. Gillis, and L. Robertson (2009), Late Quaternary eolian deposits of northern North America: Age and extent, Geological Survey of Canada, Open File 6006.
- Yoshikawa, K., and L. D. Hinzman (2003), Shrinking thermokarst ponds and groundwater dynamics in discontinuous permafrost near Council, Alaska, *Permafrost Periglacial Process.*, *14*, 151–160.
- Yvon-roucher, G., A. P. Allen, D. Bastviken, R. Conrad, C. Gudas, A. St-pierre, N. Thanh-duc, and P. A. Giorgio (2014), Methane fluxes show consistent temperature dependence across microbial to ecosystem scales, *Nature*, *507*, 488–491, doi:10.1038/nature13164.
- Zhuang, Q., J. M. Melillo, D. W. Kicklighter, R. G. Prinn, A. D. McGuire, P. A. Steudler, B. S. Felzer, and S. Hu (2004), Methane fluxes between terrestrial ecosystems and the atmosphere at northern high latitudes during the past century: A retrospective analysis with a process-based biogeochemistry model, *Global Biogeochem. Cycles*, *18*, GB3010, doi:10.1029/2004GB002239.
- Zimov, S. A., Y. V. Voropaev, I. P. Semiletov, S. P. Davidov, S. F. Prosiannikov, F. S. Chapin III, M. C. Chapin, S. Trumbore, and S. Tyler (1997), North Siberian lakes: A methane source fueled by Pleistocene carbon, *Science*, *277*, 800–802, doi:10.1126/science.277.5327.800.